Circular Directional Modulation Transmitter Array

Ding, Y., Fusco, V., & Chepala, A. (2017). Circular Directional Modulation Transmitter Array. *IET Microwaves, Antennas and Propagation*, *11*(13), 1909-1917. https://doi.org/10.1049/iet-map.2016.1140

Published in:
IET Microwaves, Antennas and Propagation

Document Version:
Peer reviewed version

Queen's University Belfast - Research Portal:
Link to publication record in Queen's University Belfast Research Portal

Circular Directional Modulation Transmitter Array

Yuan Ding, Vincent Fusco, Anil Chepala

The Institute of Electronics, Communications and Information Technology (ECIT),
Queen's University of Belfast, Belfast, United Kingdom, BT3 9DT
yding03@qub.ac.uk

Abstract: This paper proposes for the first time a directional modulation (DM) transmitter constructed using a circular array. The mode patterns, generated with the help of a Fourier transform network, are exploited in order to synthesis information patterns and orthogonal interference patterns, which enable the required DM functionality. The design procedures are presented, and example simulation results are provided. When compared with its linear DM counterpart, the proposed circular DM system exhibits enhanced secrecy performance.

1. Introduction

Directional modulation (DM) techniques are showing promise as a means to secure wireless transmission directly at the physical layer [1–5]. They have the capability of preserving the modulated signal waveforms, equivalent to the patterns of signal constellation diagrams in in-phase and quadrature (IQ) plane when digitally modulated, only along a pre-specified spatial communication direction in free space where the intended receiver locates. In the mean time, the signal waveforms radiated elsewhere are arbitrarily distorted, so that the possibility of information interception by eavesdroppers positioned off the selected secure communication direction is greatly reduced.

A number of DM array synthesis methods have been proposed so far, such as bit error rate (BER)-driven optimization-based approaches in [1, 2], radiation pattern synthesis inspired methods in [6–8], and orthogonal vector approaches in [9–11]. It was found with the orthogonal vector approaches that the DM functionality is virtually enabled by injecting artificial interference that is orthogonal to the useful information signals along the selected secure communication direction, in other words, the far-field patterns of interference radiation have power nulls directed towards the intended receiver [7, 12]. Apart from the above synthesis methods, some types of DM transmitter arrays are constructed so that no DM synthesis is required, i.e., 'synthesis-free', such as, Fourier beamforming network enabled linear DM arrays in [13, 14], retrodirective DM arrays in [15], and antenna subset modulation or 4-dimensional (4-D) arrays in [16–20]. Take 4-D DM arrays as an example, by introducing time as an additional design degree of freedom, when the number of antennas in an arbitrarily selected subset of the array, activated for each symbol transmission in free space, is fixed, then direction-dependent signal waveforms are generated. This type of array is normally studied in the frequency domain, following the approaches for analysing time-modulated arrays [21]. It concludes that when aliasing between centre frequency band and sidebands occurs, the filtered signal waveforms are distorted. This aliasing effect can only happen along directions other than the direction towards which the beam at the centre frequency band is projected. Essentially, these 4-D DM arrays can be regarded as a special realisation of the general DM concept

[22], subject to hardware constraints, such as using switches rather than array feeding networks with fully-controlled magnitudes and phases. On the other hand, the general DM concept can also be studied in the frequency domain, since we know that in order to enable DM functionality the array excitation vectors have to be updated at a rate commensurate with the symbol modulation rate, creating frequency aliasing. It is also worth noting that when we want to manipulate sidebands in 4-D DM arrays for enhanced security performance [23], then the idea of 'synthesis-free' cannot be applied.

In this paper, we say that the proposed circular DM array is 'synthesis-free'. Here the terminology 'synthesis-free' as applied to a DM architecture simply means that the secure communication direction, and the generated artificial orthogonal interference can be set and altered through the DM hardware, normally in radio frequency (RF) frontends, without the needs to mathematically calculate the array excitation vectors. It is also noted that the active element patterns of the array still need to be measured to 'calibrate' the system before transmission.

As far as the authors are aware, to date the DM research has been confined to the study of linear transmit arrays, which inevitably leads to the following fundamental problems:

- when each array antenna has an active element pattern that approximately covers half space, e.g., patch antenna or dipole over a parallel ground plane, the secured communication direction can only be selected within this half space. Commonly and unfavorably, the choice of these array elements also results in low gain when the desired transmission direction is close to the axis of the array; also when each array antenna has an isotropic active element pattern, an undesired mirroring information beam in the required beam direction with respect to the array axis would be formed, which not only wastes energy but also compromises system secrecy performance. Similar to the radiation beam, the information beam describes the main spatial region within which a receiver could successfully recover the transmitted data subject to a certain signal to noise ratio (SNR) condition;
- When the intended receiver locates close to the array axis, regardless of the choice of the antennas with half-space or isotropic active element patterns, the beamwidths of the array radiation beams, and consequently those of the resulting information beams, would be broadened, leading to a greater amount of information leaked.

It is well-known that because of symmetric arrangement circular arrays can scan beams in entire 360° with negligible variations in gain and beamwidth. Recent studies in circular or concentric ring arrays are mainly focused on synthesis of array geometries and excitations that produce predefined radiation patterns [24, 25]. It needs to be pointed out that we cannot simply replace the linear arrays in previously mentioned 'synthesis-free' DM systems [13–20] with circular arrays while maintaining DM functionality. This is because a) the Fourier networks enabled beams in [13, 14] are orthogonal in spatial domain only when the arrays are linear and half wavelength spaced; b) sum and difference patterns in [15] can only be generated with linear arrays; c) the excitation strategy in 4-D DM arrays [16–20], i.e., exciting a fixed number of antenna elements, only works when the antenna active element patterns are identical and have the same orientations which does not hold in circular arrays. In this paper, we exploit the properties of mode patterns [26] generated by circular arrays to construct 'synthesis-free' DM systems. In addition to solving the previously listed problems associated with the linear DM arrays, the proposed circular DM architecture also has some promising features;

- it is a dynamic DM transmitter, which is more secure than a static one. The definition of the dynamic and static DM systems can be found in [27];

- it is 'synthesis-free', i.e., after the system calibration, no mathematical calculation is required to set and alter the secure communication directions and the generated artificial orthogonal interference. All these are automatically achieved through the Butler matrix and the associated RF circuits;
- the secure communication direction can be continuously scanned within the whole space, unlike the Fourier beamforming network based linear DM transmitter arrays [14], where the secure communication direction can only be discretely selected within the half space;
- the DM power efficiency (PE_{DM}), which directly determines achievable DM system secrecy performance [9, 27], can be readily controlled.

In order to demonstrate these features this paper is organized as follows; In Section 2 the architecture of the proposed circular DM transmit array is described, while its operation principle and design procedures are elaborated in Section 3 through a typical example. The performance of this exemplar circular DM system is presented in Section 4 while being compared with its linear counterpart, validating the superiority of the proposed circular DM array. Finally, conclusions are drawn in Section 5.

2. Architecture of proposed circular DM transmitter

The architecture of the proposed circular DM transmitter is depicted in Fig. 1. For illustration purpose, a circular dipole array with uniform half wavelength ($\lambda/2$) spacing is adopted in Fig. 1. A metal cylindrical ground plane is added a quarter wavelength ($\lambda/4$) away from the dipole array elements. Other types of the array elements, e.g., patch antenna, can be equivalently used. The circular array is connected to the N array ports of a Fourier transform network, which, at the input end, has $N + 1$ mode ports when N is even, otherwise N mode ports when N is odd. When individual mode ports are excited, the corresponding circular array mode patterns are generated [26], as graphically illustrated in Section 3. At the mode ports an array of phase shifters ϕ_k is inserted for the purpose of steering the required information beam towards the intended receiver, the same function as those used in conventional linear phased arrays for radiation beam steering. Up to $2M+1$ ($M < N/2$) modes, excluding the highest $N-2M$ (N is even) or $N-2M-1$ (N is odd) modes, can be utilized for information transmission. Following a detailed derivation to estimate ripples on mode power patterns, a rule of thumb for the choice of M is provided in Appendix A. In addition a selection of modes is exploited for orthogonal interference injection. This is the key to enable the DM characteristic in the proposed architecture. The injected artificial interference is guaranteed, or nearly guaranteed, to be orthogonal to the radiated information signal along the selected secure communication direction by selecting some symmetrical mode pairs, i.e., positive and negative modes with the same order, each of which is fed with out-phased interference. The criteria for the choices of modes for information and orthogonal interference radiation are different, and they are elaborated in the following section. Here it should be noted that although not all the modes can be utilised for information transmission, the order of the Fourier transform network required is still N. Otherwise the desired modes cannot be properly generated [26].

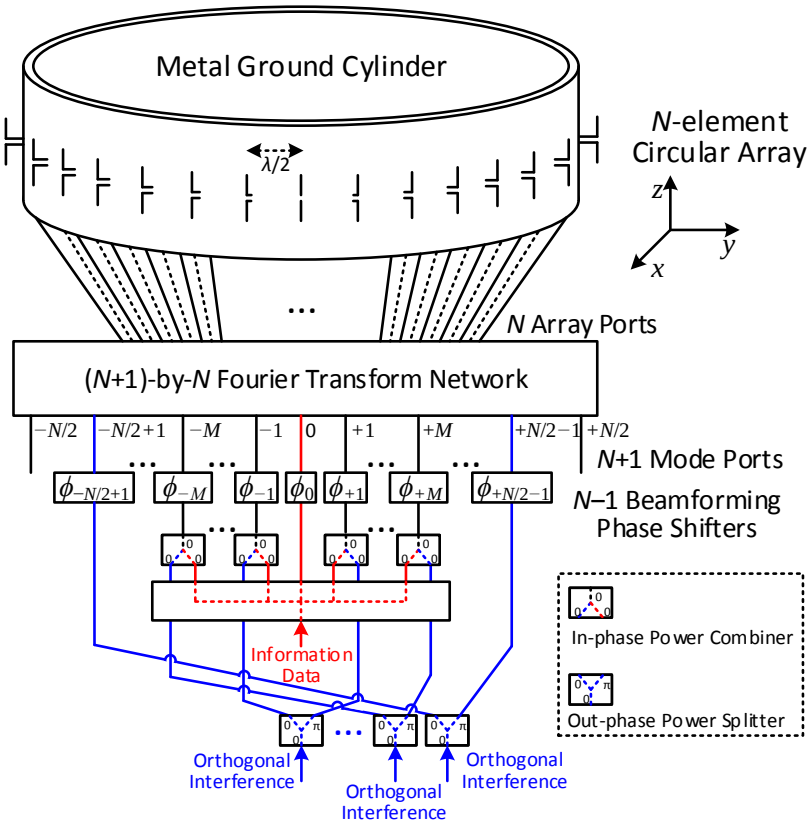

Fig. 1. *Architecture of proposed circular DM transmitter. N is assumed to be an even number.*

3. Operation principle

In this section the operation principle of the proposed circular DM architecture described earlier is discussed in details, which begins with the explanation of the mode patterns of a circular array.

In [26] it was shown that when the n^{th} antenna in an N-element circular array is excited by

$$\boldsymbol{A}_{nk} = C_k e^{2\pi kn/N}, \tag{1}$$

the k^{th} ($k \in \{-N/2, ..., +N/2\}$ when N is even, or $k \in \{-(N-1)/2, ..., +(N-1)/2\}$ when N is odd) far-field mode pattern can be generated. 'C_k' is a constant denoting the excitation magnitude at the array element port. The array excitations in (1) can be distributed using a Fourier transform network with each of its input ports corresponding to a mode pattern, thus they are labeled mode ports in Fig. 1. With this arrangement, 'C_k' becomes $B_k/\sqrt{N}$, where 'B_k' is the excitation magnitude at the k^{th} mode port, provided the Fourier transform network is lossless. In order to facilitate calculation in this paper, we set the values B_k to be identical for each k, and equal to $\sqrt{N}$, because this makes C_k unity. The use of non-uniform coefficients B_k could achieve the trade-off between main beam beamwidth and sidelobe levels, similar to what the magnitude tapering does in linear arrays. Further study on this aspect, while considering the impact of non-ideal mode patterns, is the subject for future investigation.

In order to clearly describe the operation principle of the proposed circular DM structure, a 32-element circular dipole array with a conducting ground cylinder, operating at 900 MHz, is used

as an example. All the mode patterns in x-y plane were obtained by simulation in CST Microwave Studio [28], some of which are depicted in Fig. 2. Due to the periodical array geometry, only the mode patterns within the spatial sector of 1/32 of 360° centred along the 1^{st} dipole are presented. Here we set the 1^{st} array element located along the spatial direction $\theta = 0°$. From the results shown in Fig. 2, it can be found that

- the power pattern of each mode across the space is not identical, and they are not flat, especially for the higher modes;
- two mode patterns in each pair, namely, positive and negative mode patterns with the same order, are mirror symmetrical with respect to the reference direction, i.e., $\theta = 0°$ in the example in Fig. 2, which indicates that they have identical gains and phases along this reference direction.

The above two properties are of importance when designing the proposed circular DM transmit array.

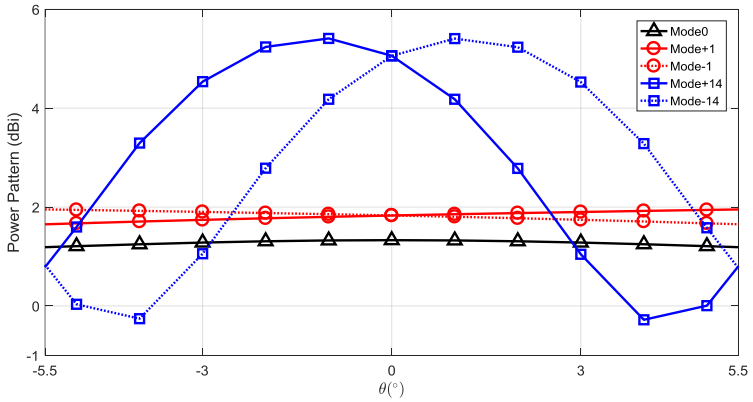

(a)

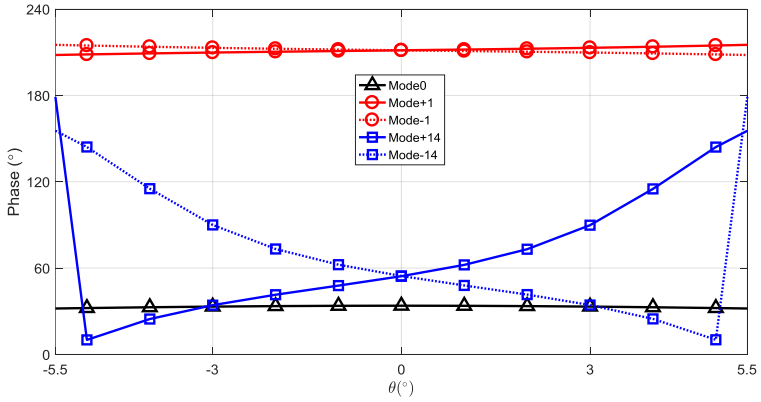

(b)

Fig. 2. *Simulated 0, ±1, and* ±14 *mode patterns ((a) power, (b) phase) in x-y plane for the example 32-element circular dipole array with a conductive ground cylinder, operating at 900 MHz. For each mode, B_k is set to be* $\sqrt{32}$.

The DM operation is now explained, first for ideal orthogonal case, then for a more general quasi-orthogonal scenario. Here 'orthogonal' or 'quasi-orthogonal' refer to the artificial interfer-

ence of 'zero power' or 'very low power (lower than −21 dB)' along the selected secure communication direction along which the useful information is projected.

A) *Ideal Orthogonal Scenario*

Remark: For an N-element circular array, there exist N discrete spatial directions along which transmitted information and artificial interference are orthogonal, i.e., an ideal DM transmitter can be constructed. These directions are

$$\alpha_l = \frac{2\pi l}{N} + \theta_{ref}, \tag{2}$$

where l is an integer ($l \in \{0, 1, ..., (N-1)\}$), and θ_{ref} is the direction where the reference antenna locates.

The above statement is explained in two steps using the example 32-element circular dipole array, namely, $N = 32$ and $\theta_{ref} = 0°$.

1. for a desired secure communication direction α_l, set the values of phase shifters at mode ports to be

$$\phi_k = \begin{cases} -\frac{2\pi l}{k} - \varphi_k(\theta_{ref}) & (k \neq 0) \\ -\varphi_k(\theta_{ref}) & (k = 0) \end{cases}. \tag{3}$$

   Here $\varphi_k(\theta_{ref})$ is the phase of the k^{th} mode pattern along θ_{ref}, e.g., those shown in Fig. 2(b) along $\theta = 0°$.

   After the phase regulation through the phase shifter array with values in (3), the generated mode patterns are phase aligned along the selected α_l, i.e., beamforming is achieved towards the desired receiver. In principle, the greater number of modes used for beamforming, the narrower the main beam will be. However, the inclusion of some higher modes with large ripples in their power patterns, see in Fig. 3 the mode power patterns for the example 32-element circular dipole array, results in undesired higher sidelobes and main beam pointing errors [29]. This aspect is demonstrated in Fig. 4(a), where the quality of the information patterns generated using modes from −10 to +10 is much better than that of the patterns generated using all modes, in terms of the main beam shape and the sidelobe levels. A slight increase or decrease of the number of utilised modes, given M is not too large, can provide trade-off between the main beam beamwidth and sidelobe levels, similar as the role that the number of antenna elements in a linear array plays on its far-field beamforming pattern. This is illustrated in Fig. 4(b), where modes up to ±9, ±10, or ±11 are activated. The trade-off between the main beam beamwidth and the first sidelobe levels can be observed. In Fig. 4(a) and Fig. 4(b), only the beam patterns directed towards α_l ($l = 0$) are depicted. For the other 31 directions α_l ($l \neq 0$), the resulting patterns are essentially identical but shifted $2\pi l/32$ in spatial domain. Thus they are omitted here.

   In Appendix A, using the same 32-element circular dipole array as an example, a detailed derivation for a newly defined figure of merit, i.e., ripples on the mode power patterns, is presented. In practice, the magnitudes of the ripples on mode patterns greatly affect the quality of the beamforming patterns, in terms of sidelobe levels and beam pointing errors. System designers can thus select the number of modes, based on the estimated ripples, usable for information beamforming according to different application requirements. There is no universally optimum choice for the number M, as the application requirements, circular array

physical arrangements, antenna elements, and mode excitation strategies can be different. But as a rule of thumb, the modes up to a few more than $\pm N/4$ can be exploited to generate information patterns. Also the more directive the active element patterns in the array, the fewer the modes should be used.

To continue the further discussion in this paper, we choose modes up to ± 10 for information transmission, i.e., $M = 10$ in Fig. 1.

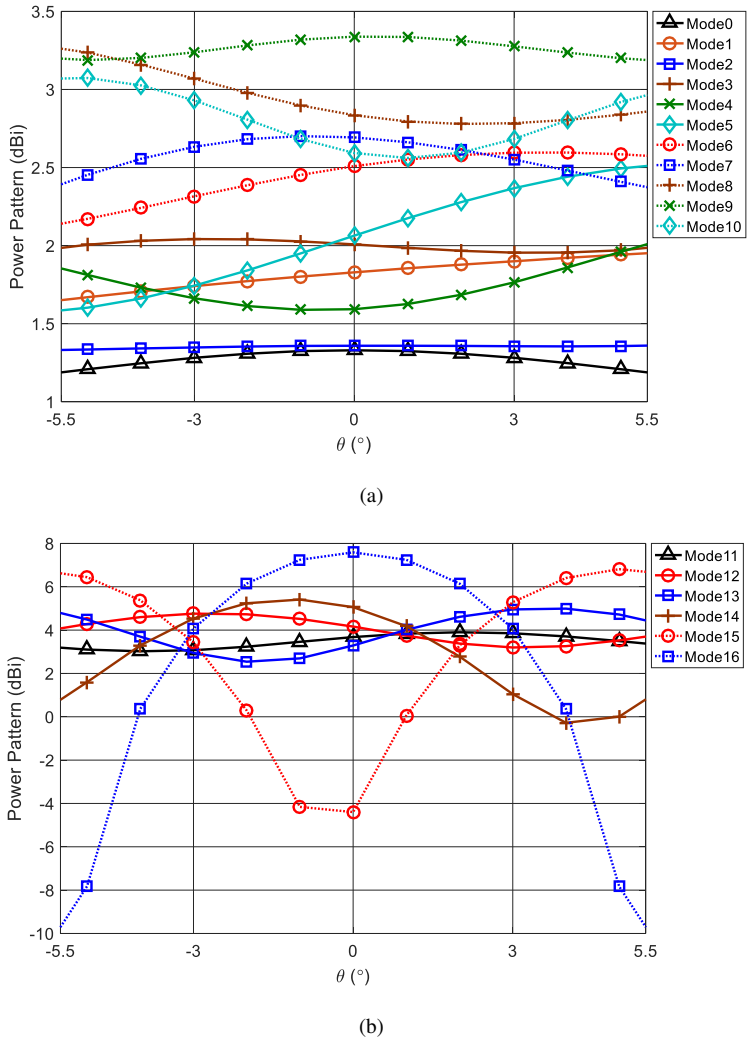

Fig. 3. *Simulated zero and all positive mode power patterns in x-y plane for the example 32-element circular dipole array with a conductive ground cylinder, operating at 900 MHz. For each mode, B_k is set to be $\sqrt{32}$.*

2. sort the mode ports into symmetrical pairs, i.e., positive and negative modes with the same order, and inject out-phased identical interference into each mode port in selected pair(s). When one of 32 α_l in (2) is selected, all the mode pairs, excluding the mode pair of the highest order, can be used to inject interference, because, as we found earlier, two mode patterns in one pair have identical magnitudes and phases along $\theta_{ref} = 0°$, which, when being out-phase excited, always give a perfect power null along the selected α_l, see Fig. 5(a). These patterns

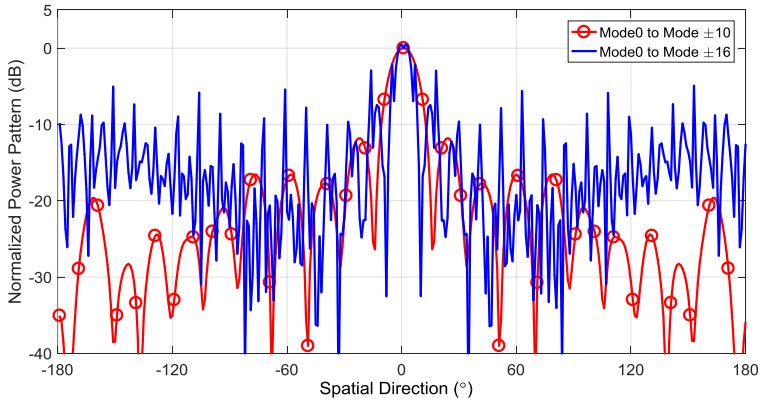

(a)

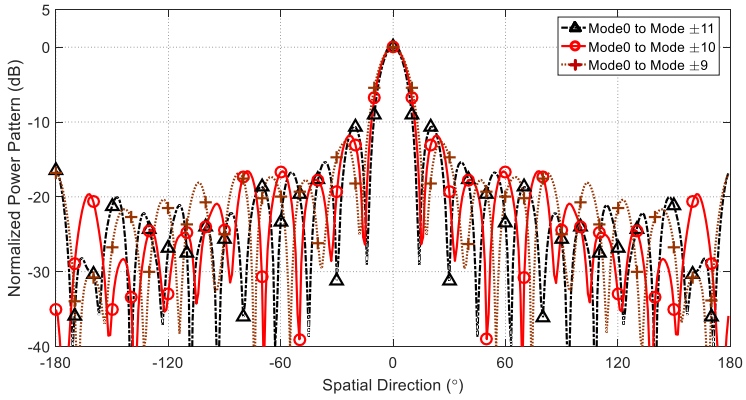

(b)

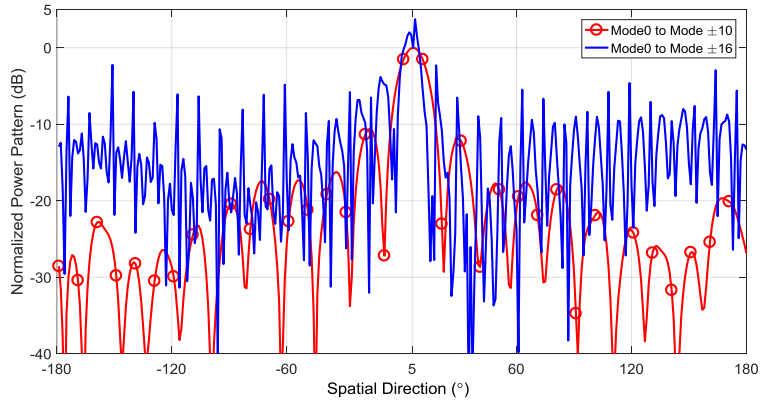

(c)

Fig. 4. *Simulated normalized beamforming power patterns when different numbers of modes are activated. The excitation magnitudes for each mode are identical.*
(a) $\alpha_0 = 0°$*, modes up to* ± 10 *or all modes are activated;*
(b) $\alpha_0 = 0°$*, modes up to* ± 9*,* ± 10*, or* ± 11 *are activated;*
(c) $\beta_0 = 5°$*, modes up to* ± 10 *or all modes are activated.*

corresponding to each mode pair are termed as interference patterns. The highest order mode pair is excluded because the two mode patterns in this pair are essentially identical in the

whole space which means no interference can be radiated when being out-phase activated.

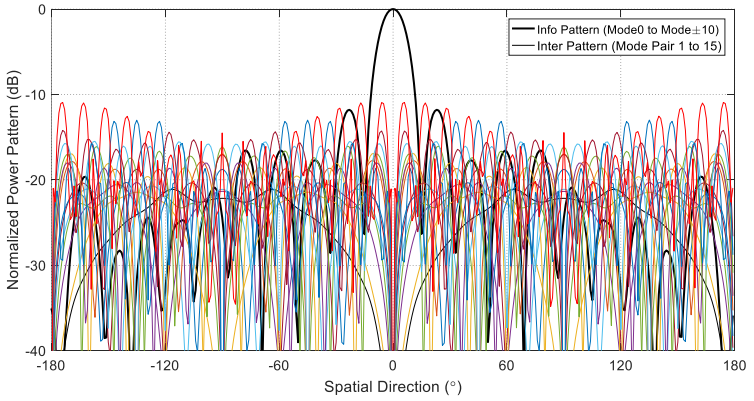

(a)

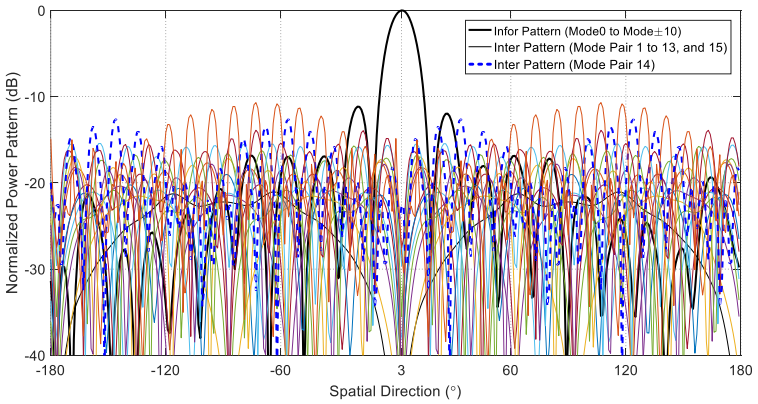

(b)

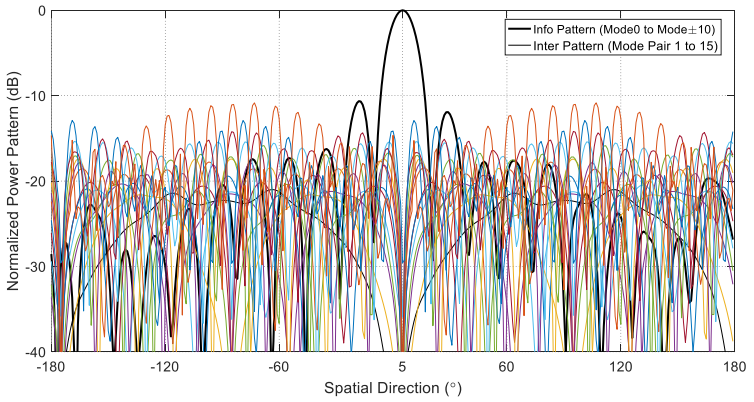

(c)

Fig. 5. *Simulated normalized information patterns, excited using modes from* -10 *to* $+10$*, and interference patterns, generated by each mode pair. The excitation magnitudes for each mode are identical. The beamforming directions, i.e., the desired secure communication directions are selected such that (a)* $\alpha_0 = 0°$*, (b)* $\beta_0 = \eta = 3°$*, and (c)* $\beta_0 = \eta = 5°$*.*

When we apply useful information on the synthesised information pattern and project random interference through interference patterns, the circular DM transmitters are constructed. For exam-

ple, Fig. 6 shows the far-field patterns when a data stream of 30 random Quadrature Phase Shift Keying (QPSK) symbols are transmitted. For each QPSK symbol, an arbitrary interference pattern out of 15 possibilities is selected for orthogonal interference projection. The power patterns are normalised such that the power along the selected communication direction, 0° in this example, is set to 0 dB. With the orthogonal interference injected, the power around 0° can thus exceed 0 dB. These far-field patterns can be viewed as received noiseless constellation patterns in IQ space at receive side along each spatial direction. As a consequence, it can be seen that the standard QPSK constellation pattern, i.e., central-symmetrical square in IQ space, can only be detected along the selected α_l.

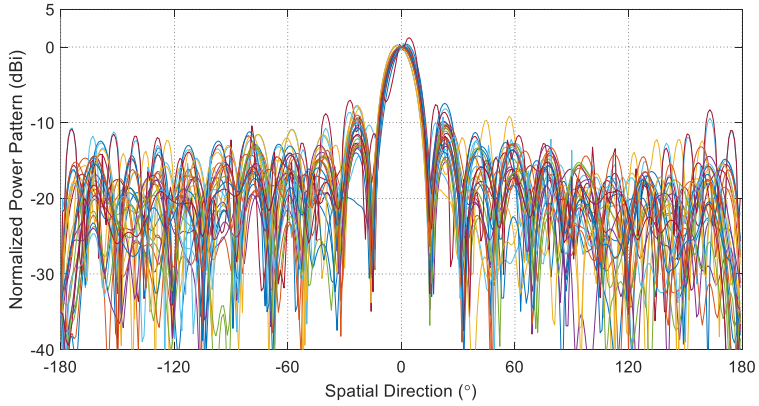

(a)

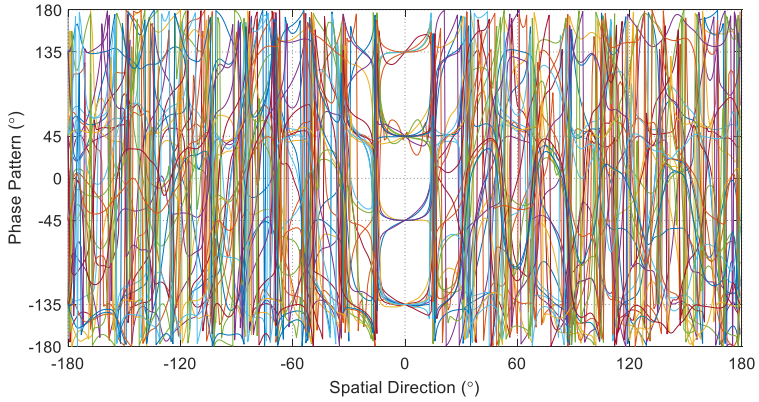

(b)

Fig. 6. *Simulated normalised patterns, both a) magnitudes and b) phases, when a data stream of 30 random QPSK symbols is transmitted. Information is conveyed through modes from* -10 *to* $+10$*, and interference is generated by a randomly selected mode pair. The excitation magnitudes at each mode port for both information and interference are set to be identical.*

B) *Quasi-Orthogonal Scenario*

When the intended secure communication direction is arbitrarily selected, denoted as β_l, such that $\beta_l \neq \alpha_l$, seen in (4),

$$\beta_l = \frac{2\pi l}{N} + \eta + \theta_{ref} \tag{4}$$

the injected interference through each mode pair can leak into the desired secure communication direction β_l. η in (4) belongs to $(-\pi/N, +\pi/N]$ and $\eta \neq 0$. Similar to the ideal orthogonal scenario, the information pattern is still synthesised using modes from -10 to $+10$, see the example in Fig 4(c) when $\beta_0 = \eta = 5^\circ$.

Fortunately, the amount of interference leaked is extremely small, see Fig. 5(b) and Fig. 5(c), where $\eta = 3^\circ$ and 5° respectively. For the example in Fig. 5(b) (or Fig. 5(c)), the greatest amount of interference leaked is only -24 dB (or -29 dB) when the 14^{th} mode pair is used for interference injection, which indicates that little impact to the desired receiver can be expected when the SNR is much lower than 24 dB (or 29 dB). This aspect will be shown in the next section. Table 1 gives the minimum signal to interference ratio (SIR) along β_l when the η is selected within $(-\pi/N, +\pi/N]$. Here it is assumed that the excitation magnitudes at each mode port for both information and interference generation are identical.

Table 1 Minimum SIR along β_l for various selected η when each mode pair is separately activated for interference injection.

$\eta(^\circ)$	maximum of SIR (dB)	Corresponding interference mode pair index
−5	29	14
−4	24	14
−3	24	14
−2	21	15
−1	21	15
1	21	15
2	21	15
3	24	14
4	24	14
5	29	14

Importantly the property of this quasi-orthogonal information and interference enables the desired secure communication directions to be continuously scanned within the entire 360°, compared with the linear Fourier DM array [14] where the directions can only be selected along some discrete spatial directions in half space.

4. Performance of circular DM transmitter

In this section the BER performance of the DM system simulated using the same 32-element circular dipole array is presented, and compared with its linear counterparts. The details of the method for BER calculation can be found in [27]. QPSK modulation with Gray-coding is adopted. A data stream consisting of 10^{+7} random symbols is generated for each BER simulation, which allows BERs down to 10^{-5} to be calculated. In each BER simulation it is assumed that the desired receiver and potential eavesdroppers are positioned the same distance away from the DM transmitter, and they experience independent additive white Gaussian noise (AWGN) with identical power. When potential eavesdroppers are positioned along every spatial directions, a BER spatial distribution can be obtained, which provides a graphic indicator of the system secrecy performance, such as the width of the main BER beam around the desired receiver direction and the levels of BER sidelobes. The cases when eavesdroppers suffer less amount of AWGN, e.g., receivers with higher sensitivity, and/or eavesdroppers are positioned closer to the transmitter, are equivalent to

the higher SNR scenarios. We deliberately choose two SNR values of 12 dB and 23 dB in the simulation, because under these scenarios the BER main beam and the first BER sidelobe reach around 10^{-4}, respectively, so that the enhancement of secrecy performance brought by the DM functionality can be readily observed.

A) *Ideal Orthogonal Scenario*

Firstly we consider 32 α_l directions in (2). In this case the perfect orthogonality between information and artificial interference can be achieved, see Fig. 5(a). This guarantees the information waveforms detected by the desired receiver uncontaminated, regardless of the amount of interference injected, i.e., BERs are kept constant along the selected α_l, see the example in Fig. 7(a) when the receiver is assumed to be positioned along $\alpha_0 = 0°$. DM Power efficiency PE_{DM} describes how much of the total radiated power, in percentage, is exploited for information transmission [27], thus PE_{DM} of 100% means no artificial interference is radiated, i.e., conventional beamforming arrays. When only one mode pair is utilized for interference input with each of its excitation magnitude being the same or twice of each of the 21 modes (only modes -10 to $+10$ are used for information beamforming, see discussions in Section 3) used for information transmission, the $PE_{DM}s$ can be calculated, respectively, to be

$$\frac{21 \times 1^2}{21 \times 1^2 + 2 \times 1^2} \times 100\% = 91.3\% \tag{5}$$

and

$$\frac{21 \times 1^2}{21 \times 1^2 + 2 \times 2^2} \times 100\% = 72.4\%. \tag{6}$$

Lower PE_{DM} means more artificial interference is radiated, generally leading to more enhanced security performance. In this sense, there is a trade-off between the total energy radiated and the achievable security performance. When the requirement of system security performance is set, the optimum PE_{DM} can be accordingly determined through simulation.

In relatively low SNR condition, the BER sidelobes remain high even in the conventional beamforming array, see the solid curve in Fig. 7(a) for SNR of 12 dB. While in order to effectively narrow the BER main beam, a mode pair with a power dip along $\theta_{ref} = 0°$ in the corresponding mode patterns, i.e., the mode pair 15 (see Fig. 3(b)), should be selected for orthogonal interference injection, since this type of mode patterns can deliver greater amount of interference power into the spatial regions close to the desired secure communication direction. Also as we can expect, greater interference power (lower PE_{DM}) leads to narrower BER main beams, as illustrated in Fig. 7(a), i.e., the beamwidth for BER lower than 10^{-2} reduces by two thirds (from 18° to 6°) when PE_{DM} is lowered from 100% to 72.4%.

When the SNR is high, e.g., SNR of 23 dB in Fig. 7(b), the levels of BER sidelobes in the conventional beamforming array ($PE_{DM} = 100\%$) can be low, especially for two first sidelobes, which poses high risk of information being intercepted. Increasing the interference power radiated through a selected mode pair can eliminate most BER sidelobes. However, there are some sidelobes that are not sensitive to interference, e.g., the sidelobes around ±60° when the mode pair 6 is selected to radiate interference, see Fig. 7(b), because along these directions the two mode patterns in the pair are almost identical, e.g., $1.97\angle 91°$ for mode 6 and $2.3\angle 96°$ for mode -6 along the direction 60°, resulting in little interference being projected along these directions (since two mode ports in a pair are out-phase excited by the interference). In order to avoid these

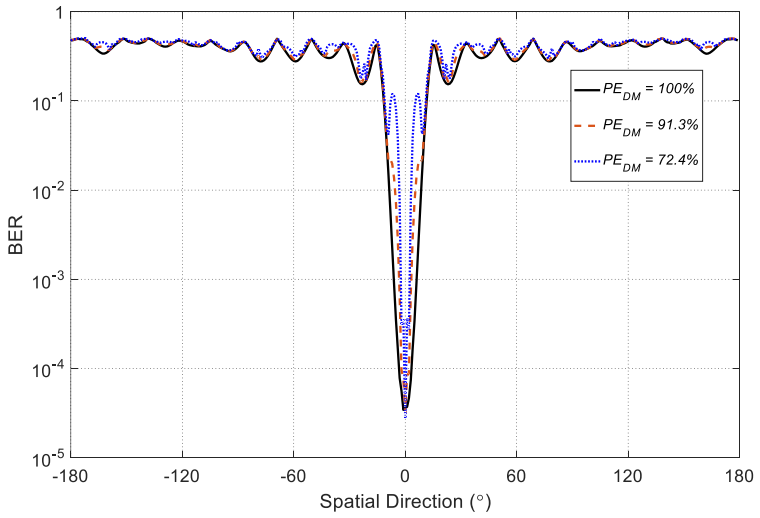

(a)

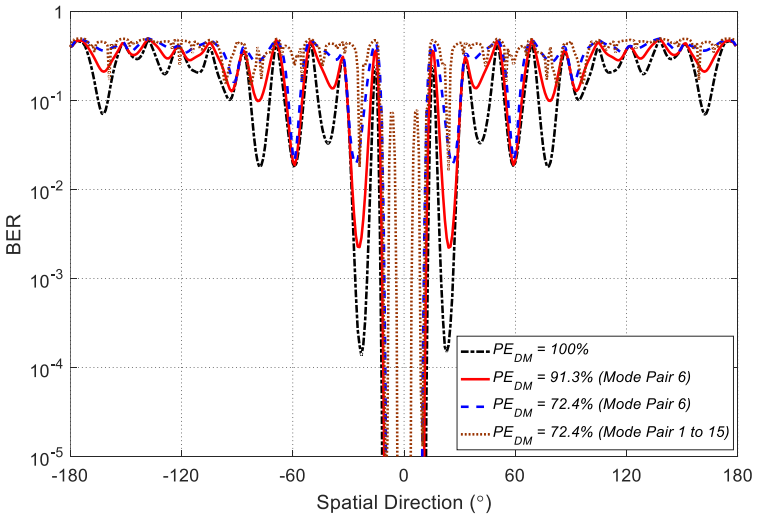

(b)

Fig. 7. *Simulated BER spatial distribution when* $\alpha_0 = 0°$.
a The mode pair 15 is used for orthogonal interference injection, and SNR along $\alpha_0 = 0°$ is assumed to be 12 dB;
b SNR along $\alpha_0 = 0°$ is assumed to be 23 dB.

'*interference-insensitive*' directions, the interference energy should be spread out among all available mode pairs, which is evidenced by the dotted curve in Fig. 7(b).

B) *Quasi-Orthogonal Scenario*

Secondly we consider the more general case when the intended secure communication is β_l in (4). In this case the information and artificial interference are not ideally orthogonal. We choose $\eta = 3°$ and $l = 0$ as an example. The system BER spatial distributions were simulated and some of them are plotted in Fig. 8. In order to investigate the effect of the leaked interference on the information recovery along the intended receiver, the worst case along $\beta_l = 3°$, i.e., injecting

interference through the mode pair 14, is presented in Fig. 8(a) for different PE_{DM}s when SNR is assumed to be 12 dB. It can be concluded that the information and interference can be considered as quasi-orthogonal when SNR is much lower than the SIR (SNR = 12 dB $\ll$ SIR = 24 dB), i.e., the system is noise-limited. This means that unlike the linear Fourier DM arrays [14] the secure communication direction can be continuously scanned within the entire 360°.

To observe the BER sidelobes, we increase the SNR along $\beta_l = 3°$ to 23 dB in Fig. 8(b). Similarly, the same as what we found in the first case, greater amount of interference power helps reduce BER sidelobes, and evenly spreading the interference energy among all available mode pairs can achieve further sidelobe reduction. It is noted that the BER along this $\beta_l = 3°$ are expected to be deteriorated since the SNR of 23 dB is comparable with the maximum SIR of 24 dB when the mode pair 14 is selected for interference injection. However, this high SNR region is not commonly used in practical systems. Even if the high SNR is required, we can exclude the mode pair 14 to further extend the system noise-limited region.

C) *Comparison Between Circular and Linear DM Systems*

Finally the BER spatial distributions of the proposed circular DM system is compared with those of its linear counterpart. The counterpart used for comparison in this subsection is a linear $\lambda/2$ uniformly spaced DM array with the same number of antenna elements, i.e., $N = 32$, which, we assume, are $\lambda/2$ dipoles, operating at 900 MHz.

In Fig. 9 the full-wave simulated radiation patterns that are used for conveying information in both circular and linear DM arrays are shown. For the 32-element circular dipole array, mode patterns from -10 to $+10$ are used for information beamforming as we discussed in Section 3. Since circular array radiation patterns change very little when scanning the beamforming directions, seen in Fig. 5, only the pattern with main beam pointing to $\alpha_0 = 0°$ is plotted for the circular array. While for the 32-element linear dipole array, three beamforming directions, $\gamma = 0°$ (boresight), $\gamma = 25.5°$, and $\gamma = 78.5°$ (close to the array axis), are chosen. In order to facilitate comparison, the beamforming directions of all the patterns are spatially shifted and aligned along 0° in Fig. 9. From Fig. 9, it can be seen that a) when the secure communication direction γ is around boresight of the linear array, the radiation main beam for information transmission is narrower than that of its circular counterpart, while it is getting much wider when the γ is around the linear array axis. When $\alpha_0 = \gamma = 0°$ the linear array has a gain 9 dB higher, this is because the linear array has a larger 1-D aperture size and some modes in the circular array are not used for beamforming; b) the main beam gain in the linear array reduces as γ sweeps away from boresight, e.g., from 29 dBi when $\gamma = 0°$ to 18 dBi when $\gamma = 78.5°$; and c) a mirroring beam always presents in the linear array. On the contrary, the circular array with the same number of antenna elements is able to provide a nearly-unchanged beamforming pattern over the entire 360°, although with some gain loss and a little widened main beam when compared with the linear array for near-boresight communications.

Fig. 10 compares the simulated BER distributions in both circular and linear DM systems. For fair comparison, PE_{DM}s are both set to 72.4% and SNRs along their respect communication directions are assumed to be identical, first 12 dB, and then 23 dB. For the circular DM, the mode pair 15 is selected for orthogonal interference injection, as used in Fig. 7(a). While for the linear DM array, the orthogonal vector DM synthesis approach described in [9] is adopted. It can be seen that the linear DM systems may enjoy slightly narrower BER main beams when the secure communication directions γ are around boresight of the array. However, when considering much more broadened BER beams for larger values of γ and the mirroring information beams in the linear DM systems, the proposed circular DM system provides more consistent and, in general, better secrecy performance.

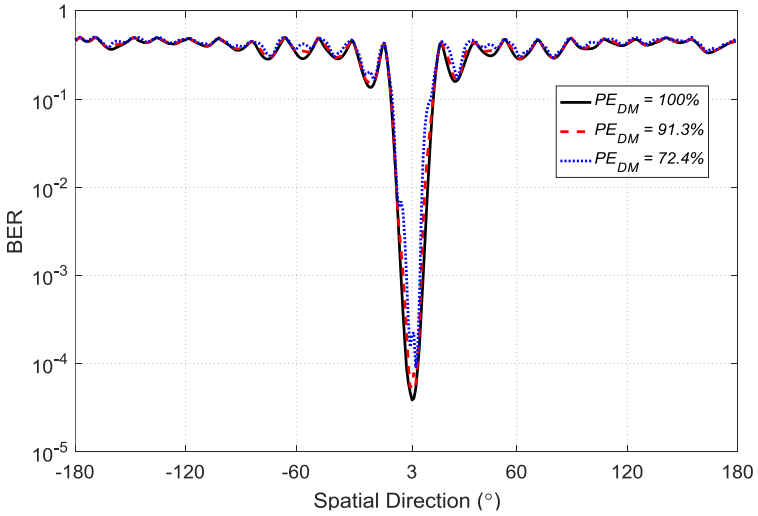

(a)

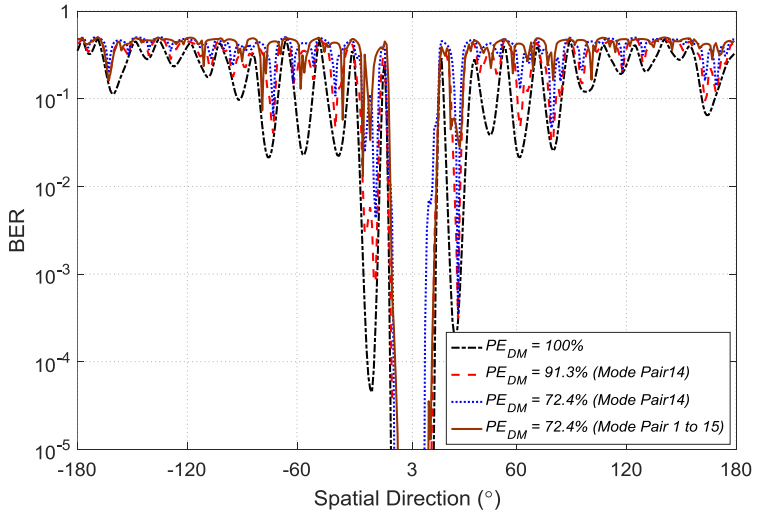

(b)

Fig. 8. *Simulated BER spatial distribution when* $\beta_l = 3°$.
a The mode pair 14 is used for orthogonal interference injection, and SNR along $\beta_l = 3°$ is assumed to be 12 dB;
b SNR along $\beta_l = 3°$ is assumed to be 23 dB.

5. Conclusion

Circular DM transmitter arrays were described in this paper. They were synthesised using the concept of mode patterns, which were generated using a Fourier transform network. The design procedures were elaborated using a typical 32-element circular dipole array, and its secrecy performance was simulated and compared with that of a linear DM array. It was shown that the circular DM system was able to provide a narrow BER main beam, irrespective of the desired secure communication directions, while in the linear DM system there existed two mirroring BER main beams, the beamwidth of which was greatly broadened when the selected secure communication

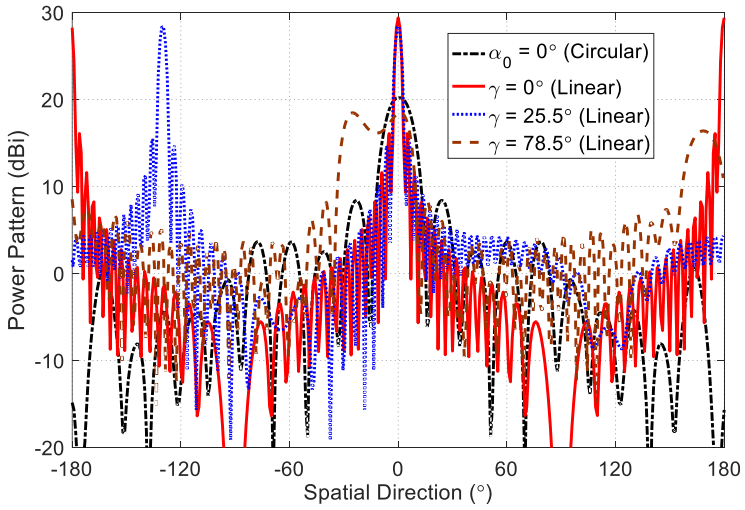

Fig. 9. *Simulated information patterns in both circular and linear DM arrays.*

directions were close to the linear array axis. The proposed circular DM transmitter array is more suitable for physical-layer secure wireless transmissions where communication nodes can move within the entire 360° spatial direction range with respect to the DM transmitter.

Appendix *A*

In this appendix, we define a figure of merit to quantify the ripples on the mode power patterns, in order to provide a guideline on how many modes can be selected to generate information beams. A detailed derivation and discussion referenced to the 32-element circular dipole array used throughout this paper are now presented.

For a circular array, the normalised far-field m^{th} mode pattern $F_m(\theta)$ can be expressed as [30]

$$F_m(\theta) = \frac{I_m}{2\pi} S(\theta) \int_0^{2\pi} G(\theta - \phi) e^{j[\beta r cos(\theta-\phi)+m\phi]} d\phi, \tag{A1}$$

where I_m is the magnitude of the current excitation for the m^{th} mode, $G(\theta)$ refers to the active element pattern in the array, $\beta = 2\pi/\lambda$ is wavenumber in free space, and r denotes the radius of the circular array, i.e., 5.1π in the example 32-element circular array. $S(\theta)$ is a sampling function which has a unit impulse at the element. It can be written as [30]

$$S(\theta) = 1 + \sum_{q=1}^{\infty} (e^{jqN\theta} + e^{-jqN\theta}). \tag{A2}$$

The active element pattern $G(\theta)$ can be considered as a periodic function with a period of 2π, therefore it can be expressed as

$$G(\theta) = \sum_{p=-P}^{+P} D_p e^{jp\theta}. \tag{A3}$$

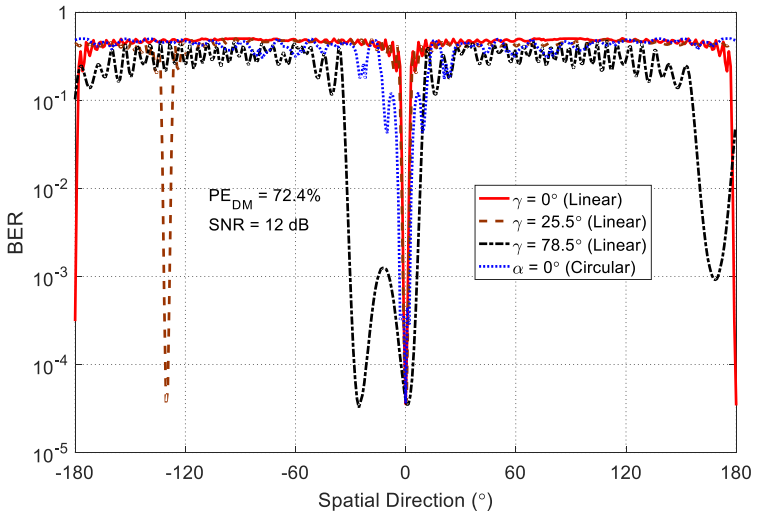

(a)

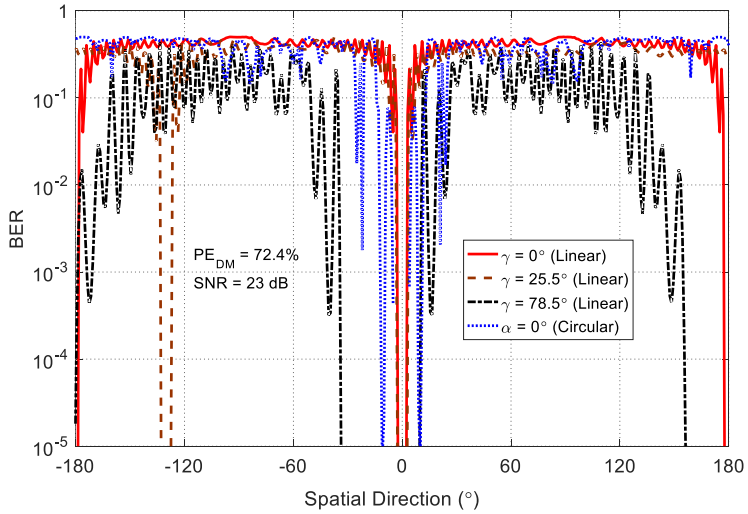

(b)

Fig. 10. *Simulated BER distributions in both circular and linear DM systems for different secure communication directions. PE_{DM}s are set to 72.4% and SNRs along their respect communication directions are assumed to be (a) 12 dB and (b) 23 dB.*

The more directive the pattern $G(\theta)$, the larger P it is required subject to a fixed fitting error. For the dipole antenna in the example circular array, the simulated active element pattern and the fitting pattern using (A3) when $P = 2$ are shown in Fig. 11. The calculated coefficients in (A3) are: $D_0 = 3.19$, $D_{\pm 1} = -2.01$, and $D_{\pm 2} = 1.41$.

Substituting (A2) and (A3) into (A1), and using the relationship

$$j^m J_m(\beta r) = \frac{1}{2\pi} \int_0^{2\pi} e^{j(mx+\beta r \cos x)} dx, \tag{A4}$$

we get

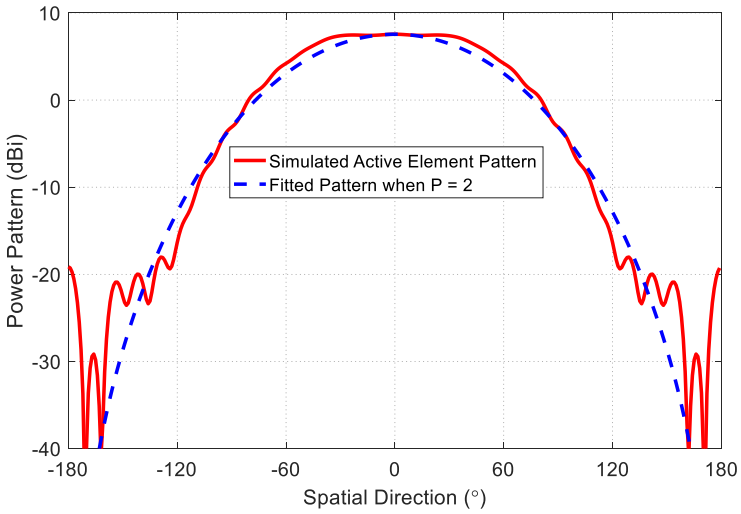

Fig. 11. *Simulated active element pattern of the dipole in the example 32-element circular array and its fitted pattern when* $P = 2$.

$$F_m(\theta) = I_m e^{jm\theta} \sum_{p=-P}^{+P} D_p j^{m-p} J_{m-p}(\beta r)$$
$$+I_m \sum_{q=1}^{\infty} \left(e^{j(qN+m)\theta} \sum_{p=-P}^{+P} D_p j^{qN+m-p} J_{qN+m-p}(\beta r) + e^{-j(qN-m)\theta} \sum_{p=-P}^{+P} D_p j^{-qN+m-p} J_{-qN+m-p}(\beta r) \right). \tag{A5}$$

$J_x(\beta r)$ in (A4) and (A5) is the Bessel function of the first kind for the order x. When x is an integer, which is the case for the discussion in this paper, $J_{-x}(\beta r) = (-1)^x J_x(\beta r)$.

The first term in the right hand side in (A5) is the desired m^{th} mode that has a constant magnitude over the entire 2π range. While the second term, which is the superposition of unwanted modes, such as $N \pm m$, $2N \pm m$, etc., distorts the desired m^{th} mode, generating ripples on the power pattern. For the example 32-element circular array where $\beta r \approx 5.1\pi$, from the property of the Bessel function shown in Fig. 12, we can conclude that all unwanted modes are determined by the Bessel functions with their orders in the decaying region. As a consequence, the dominant distortion comes from mode $(-N + m)$ when m is positive, or $(N + m)$ when m is negative. Since mode pairs are symmetric, only the positive modes are studied here.

The magnitude of the desired mode m and the dominant distortion mode $(-N + m)$ are, respectively, denoted as

$$A_m = \left| I_m e^{jm\theta} \sum_{p=-P}^{+P} D_p j^{m-p} J_{m-p}(\beta r) \right|, \tag{A6}$$

and

$$B_m = \left| e^{-j(N-m)\theta} \sum_{p=-P}^{+P} D_p j^{-N+m-p} J_{-N+m-p}(\beta r) \right|$$

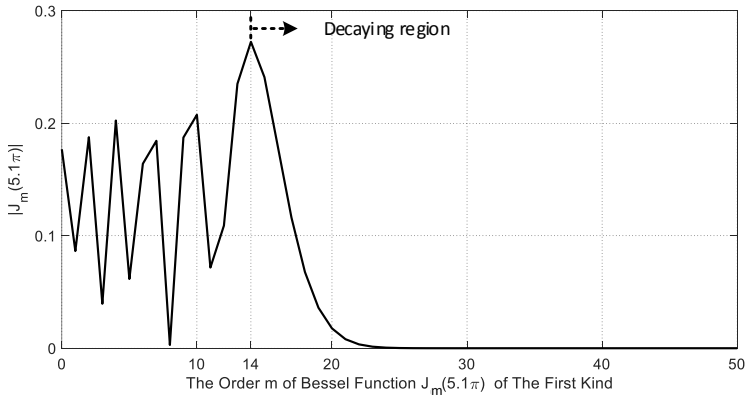

Fig. 12. *The absolute value of the Bessel function $J_m(\beta r)$ of the first kind versus its order m when $\beta r = 5.1\pi$.*

$$= \left| e^{-j(N-m)\theta} \sum_{p=-P}^{+P} D_p (-1)^{N-m+p} j^{-N+m-p} J_{N-m+p}(\beta r) \right|. \tag{A7}$$

When $m \neq |-N+m|$, both the in-phase and out-phase combinations between the m^{th} and the $(-N+m)^{th}$ modes occur within 2π region. Thus the figure of merit that quantifies the magnitude ripple in dB for the m^{th} mode can be defined as

$$R_m = 20 \times \log_{10} \left| \frac{A_m + B_m}{A_m - B_m} \right|. \tag{A8}$$

In Fig. 13 the calculated R_m for the example 32-element circular dipole array is plotted as a function of m. These results are validated when they are compared with the simulated mode patterns presented in Fig. 3, especially for those higher order modes, e.g., mode 11 and mode 15 have ripples around 1 dB and 10 dB, respectively. Some discrepancies exist for the lower order modes. These are mainly due to the value of P that is set when fitting the active element pattern in (A3). It is also pointed out that for active element patterns with higher directivity, the value of P needs to be increased to reduce the pattern fitting errors. This leads to higher ripples for the same mode order when compared with their counterparts in the circular array with less directive active element patterns. This conclusion is obtained because the dominant term $J_{N-m-P}(\beta r)$ increases as P increases in the largest distortion mode in (A7).

In practice, with the knowledge of a circular array physical arrangement and its measured active element pattern, following the procedures presented in this Appendix, the ripples in the power pattern for the m^{th} mode can be estimated. Thus a designer can determine the number of modes that are usable, in order to meet the mainlobe and sidelobe requirements for various applications. Here a rule of thumb is that modes up to a few more than $\pm N/4$ can be exploited for information beam generation, which normally provides a good trade-off among the beam shape, main beam beamwidth, and sidelobe levels.

Acknowledgments

This work was supported by the UK EPSRC under grants no. EP/P000673/1 and EP/N020391/1.

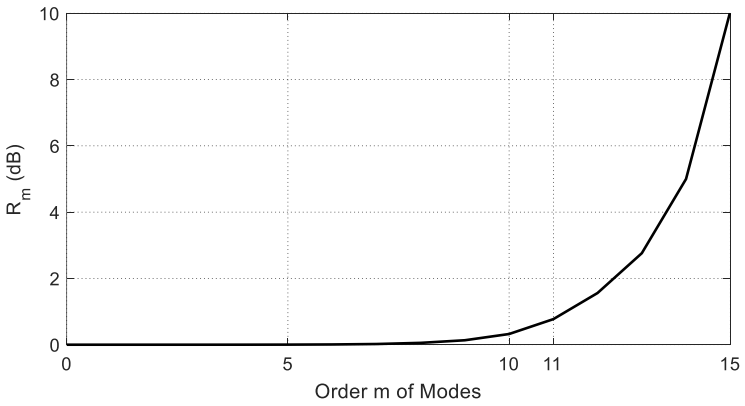

Fig. 13. *Ripple R_m calculated using (A8) for the example 32-element circular dipole array.*

References

[1] Daly, M. P., Bernhard, J. T.: 'Directional modulation technique for phased arrays', IEEE Trans. Antennas Propag., 2009, **57**, (9), pp. 2633–2640

[2] Ding, Y., Fusco, V.: 'BER-driven synthesis for directional modulation secured wireless communication', Int. J. Microw. Wireless Technol., 2014, **6**, (02), pp. 139–149

[3] Shi, H., Tennant, A.: 'Simultaneous, multichannel, spatially directive data transmission using direct antenna modulation', IEEE Trans. Antennas Propag., 2014, **62**, (1), pp. 403–410

[4] Ding, Y., Fusco, V.: 'A review of directional modulation technology', Int. J. Microw. Wireless Technol., 2015, pp. 1–13

[5] Narbudowicz, A., Heberling, D., Ammann, M. J.: 'Low-cost directional modulation for small wireless sensor nodes', Proc. 10th Eur. Conf. Antennas Propag., Davos, Switzerland, Apr. 2016, pp. 1–3

[6] Ding, Y., Fusco, V.: 'Constraining directional modulation transmitter radiation patterns', IET Microw., Antennas Propag., 2014, **8**, (15), pp. 1408–1415

[7] Ding, Y., Fusco, V.: 'Directional modulation far-field pattern separation synthesis approach', IET Microw., Antennas Propag., 2015, **9**, (1), pp. 41–48

[8] Zhang, B., Liu, W., Gou, X.: 'Compressive sensing based sparse antenna array design for directional modulation', IET Microw., Antennas Propag., 2017, **11**, (5), pp. 634–641

[9] Ding, Y., Fusco, V.: 'A vector approach for the analysis and synthesis of directional modulation transmitters', IEEE Trans. Antennas Propag., 2014, **62**, (1), pp. 361–370

[10] Hu, J., Shu, F., Li, J.: 'Robust synthesis method for secure directional modulation with imperfect direction angle', IEEE Commun. Lett., 2016, **20**, (6), pp. 1084–1087

[11] Ding, Y., Fusco, V.: 'Orthogonal vector approach for synthesis of multi-beam directional modulation transmitters', IEEE Antennas Wireless Propag. Lett., 2015, **14**, pp.1330–1333

[12] Goel, S., . Negi, R.: 'Guaranteeing secrecy using artificial noise', IEEE Trans. Wireless

Commun., 2008, **7**, (6), pp. 2180–2189

[13] Zhang, Y., Ding, Y., Fusco, V.: 'Sidelobe modulation scrambling transmitter using Fourier rotman lens', IEEE Trans. Antennas Propag., 2013, **61**, (7), pp. 3900–3904

[14] Ding, Y., Zhang, Y., Fusco, V.: 'Fourier rotman lens enabled directional modulation transmitter', Int. J. Antennas Propag., 2015, **2015**

[15] Ding, Y., Fusco, V.: 'A synthesis-free directional modulation transmitter using retrodirective array', IEEE J. Sel. Topics Signal Process., 2017, **11**, (2), pp. 428–441

[16] Hong, T., Song, M. Z., Liu, Y.: 'RF directional modulation technique using a switched antenna array for physical layer secure communication applications', Progress in Electromagn. Res., 2011, **120**, pp. 195–213

[17] Rocca, P., Zhu, Q., Bekele, E. T., Yang, S., Massa, A.: '4-D arrays as enabling technology for cognitive radio systems', IEEE Trans. Antennas Propag., 2014, **62**, (3), pp. 1102–1116

[18] Valliappan, N., Lozano, A., Heath, R. W.: 'Antenna subset modulation for secure millimeter-wave wireless communication', IEEE Trans. Commun., 2013, **61**, (8), pp. 3231–3245

[19] Zhu, Q., Yang, S., Yao, R., Nie, Z.: 'Directional modulation based on 4-D antenna arrays', IEEE Trans. Antennas Propag., 2014, **62**, (2), pp. 621–628

[20] Alotaibi, N., Hamdi, K. A.:'Switched phased-array transmission architecture for secure millimeter-wave wireless communication', IEEE Trans. Commun., 2016, **64**, (3), pp. 1303–1312

[21] Wang, W., So, H. C., Farina, A.: 'An overview on time/frequency modulated array processing', IEEE J. Sel. Topics Signal Process., 2017, **11**, (2), pp. 228–246

[22] Ding, Y., Fusco, V.: 'Development in directional modulation technology', Forum for Electromagn. Res. Methods and Appl. Technol. (FERMAT), 2016, **13**, pp. 1–7

[23] Hannan, M. A., Poli, L., Rocca, P., Massa, A.: Pulse sequence optimization in time-modulated arrays for secure communications', Int. Symp. Antennas and Propagation Society, APSURSI16, IEEE, 2016, pp. 695-696

[24] Carlin, M., Oliveri, G., Massa, A.: 'Hybrid BCS-deterministic approach for sparse concentric ring isophoric arrays', IEEE Trans. Antennas Propag., 2015, **63**, (1), pp. 378–383

[25] Bucci, O. M., Pinchera, D.: 'A generalized hybrid approach for the synthesis of uniform amplitude pencil beam ring-arrays', IEEE Trans. Antennas Propag., 2012, **60**, (1), pp. 174–183

[26] Sheleg, B.: 'A matrix-fed circular array for continuous scanning', Proc. IEEE, 1968, **56**, (11), pp. 2016–2027

[27] Ding, Y., Fusco, V.: 'Establishing metrics for assessing the performance of directional modulation systems', IEEE Trans. Antennas Propag., 2014, **62**, (5), pp. 2745–2755

[28] CST Microwave Studio Computer Simulation Technology, version 2016.

[29] Toh, B. Y., Fusco, V., Buchanan, N.: 'Assessment of performance limitations of PON retrodirective arrays', IEEE Trans. Antennas Propag., 2002, **50**, (10), pp. 1425–1432

[30] Rahim T.: 'Directional pattern synthesis in circular arrays of directional antennas', PhD thesis, Department of Electronic and Electrical Engineering, University College London, Aug. 1980